Journal of Mechanical and Construction Engineering, 2025,
Vol. 05, Iss. 01, S. No. 083, pp. 1-15
ISSN (Online): 2583-0619

Design and Development of 3KGF Thrust Stand

Paramjyot G K Tiwana[1], Pravin Kumar Singh[2]

[1] Scholar, Department of Aerospace Engineering, Amity University, Lucknow UP, India - 226008
[2] Assistant Professor, Department of Mechanical Engineering, Amity University, Lucknow UP, India - 226008
[1] paramjyot.tiwana1@s.amity.edu, [2]pravin.singh2@s.amity.edu

How to cite this paper: P. G. K. Tiwana and P. K. Singh, "Design and Development of 3KGF Thrust Stand," *Journal of Mechanical and Construction Engineering (JMCE), Vol. 05, Iss. 01, S. No. 083,* pp. 1–15, 2025.

https://doi.org/10.54060/a2zjournals.jmce.83

Received: 07/01/2025
Accepted: 09/03/2025
Online First: 25/04/2025
Published: 25/04/2025

Copyright © 2025 The Author(s).
This work is licensed under the Creative Commons Attribution International License (CC BY 4.0).
http://creativecommons.org/licenses/by/4.0/

Open Access

Abstract

This paper presents the design and development of a cost-effective, modular thrust stand capable of measuring up to 3 kgf of static thrust, tailored for testing electric propulsion systems in UAVs and drones. Utilizing accessible components like a 3 kg load cell, HX711 amplifier, 30A Hall effect sensor, and ESP8266 microcontroller, the system enables real-time wireless data acquisition for thrust, current, and power metrics. Ideal for academic and small-scale aerospace setups, the stand supports live monitoring, is easily modifiable, and lays the groundwork for advanced future testing such as torque, temperature, and multi-axis force analysis.

Keywords

Unmanned Aerial System (UAV), Thrust Stand.

1. Introduction

With the rapid growth of UAV technologies and the increasing reliance on electric propulsion, precise ground-based testing methods have become essential. Thrust stands offer a controlled environment to evaluate propulsion components, enabling

optimization of flight performance, energy consumption, and design efficiency. This paper presents the development of a compact, modular thrust stand tailored for small UAV systems, focusing on accessibility, real-time telemetry, and expandability for future enhancements.

2. Research background overview:

Al-Qutub et al. (2012) developed a thrust stand for micro gas turbines, focusing on thermal isolation and vibration damping to improve measurement accuracy. Using a strain gauge-based load cell and static calibration with known masses, they ensured linear performance across expected thrust ranges. Their work is relevant for validating high-speed propulsion systems under thermal and mechanical stress.

Duarte et al. (2018) designed a compact, strain gauge-based thrust stand for electric propulsion. They emphasized accurate calibration through polynomial regression and used FEA to minimize deflection. EMI shielding was included to enhance data reliability. Their setup is particularly suitable for low-thrust electric UAV systems.

Hoffmann et al. (2007) created a quadrotor UAV testbed to study autonomous control. While focused on flight dynamics, their system enabled accurate thrust estimation through sensor fusion and real-time telemetry. This control-centric approach supports indirect validation of thrust and power data during flight.

Leishman (2006) provides foundational theory on rotor aerodynamics, including momentum theory, blade element analysis, and low Reynolds number effects. His work informs key metrics like thrust efficiency and induced power loss, offering critical insight into interpreting small-scale rotor performance in thrust stand experiments.

Haag et al. (1991) developed a thrust stand for high-power electric propulsion devices with high precision force sensors capable of resolving minute thrust changes. The design emphasized vibration isolation and thermal shielding to maintain accuracy, making it suitable for laboratory testing of ion and plasma thrusters.

Novotňák et al. (2022) presented a modular system designed to measure key UAV performance parameters such as thrust, voltage, current, and RPM. The system incorporated real-time data acquisition and a user-friendly interface, offering a cost-effective solution for UAV diagnostics and academic research.

Jain et al. (2020) focused on designing a two-axis rocket motor thrust stand with thrust vectoring capabilities. The system was developed for static fire testing and used sensors and actuators for pitch and yaw control analysis. It demonstrated robust data collection and control mechanisms for rocket motor characterization.

Byun et al. (2018) proposed a thrust control loop design for electric-powered UAVs, where the motor-propeller system was modeled dynamically. The study implemented a feedback control algorithm that maintained steady thrust under varying flight conditions, improving UAV stability and efficiency.

Ketsdever et al. (2008) introduced a micromass balance-based thrust stand tailored for low-thrust propulsion systems like micro- and nano-sat thrusters. Their setup was capable of measuring thrusts in the micronewton range and emphasized ultra-precision force sensing, marking a significant step forward.

3. Material and Component Properties

Each component in the thrust stand system is selected to meet mechanical and electrical demands under real-world testing conditions. Below are the key specifications and operating principles:

i. **Polycarbonate Panels**

Polycarbonate is used for the thrust stand frame due to its strength and versatility:

a. Tensile Strength: ~70 MPa

b. Impact Resistance: ~900 J/m

c. Thermal Stability: Maintains properties under moderate heat and load.

d. Machinability: Easily cut and customized for sensor mounts and cable routing.

ii. **Load Cell**

A 3 kg-capacity strain gauge load cell measures thrust with the following characteristics:

a. Sensitivity: ~1 mV/V.

b. Construction: Anodized aluminum for linear response and low hysteresis.

c. Principle: Uses a Wheatstone bridge to detect strain-induced resistance changes.

d. Input Voltage: Powered by 5V from the BEC.

iii. **HX711 Amplifier**

The 24-bit HX711 ADC digitizes the load cell's signal with the following features:

a. Gain Settings: Programmable at 32, 64, or 128 (typically set to 128).

b. Output Formula:

$$\text{Output Voltage} = \text{Gain} \times (V^{+} - V^{-})$$

c. Features: Differential inputs and internal clocking for noise reduction

d. Input Voltage: 5V regulated from the BEC.

iv. **Hall Effect Current Sensor**

The Hall Effect sensor measures motor current via magnetic field detection:

a. Principle: Produces a voltage proportional to magnetic field strength around the conductor.

b. Hall Voltage Formula:

$$V_H = (I \times B) / (q \times n \times d)$$

Where:

I = current, B = magnetic field strength

q = electric charge, n = carrier density

d = sensor thickness

c. Input Voltage: Operates at 3.7V, powered by the ESP8266's 3.3V regulated output.

v. **ESP8266 Microcontroller**

The ESP8266 serves as the core processor for data handling and telemetry:

a. CPU: 32-bit Tensilica running at 80/160 MHz.

b. Features: Integrated Wi-Fi, 10-bit ADC, PWM, I2C, GPIOs.

c. Input Voltage: Powered by 5V from the BEC, internally regulated to 3.3V.

d. Function: Acquires data from the HX711 and current sensor, processes it, and transmits wirelessly.

vi. **Power Architecture**

a. A 12V input (from a LiPo or bench supply) is stepped down by a Battery Eliminator Circuit (BEC) to 5V.

b. This regulated 5V powers the load cell, HX711, and ESP8266 board.

c. The Hall Effect sensor receives 3.7V directly from the ESP8266's onboard regulator.

4. Integration of the System

The system integration was carried out in a modular and reliable manner to ensure mechanical rigidity, sensor accuracy, and ease of future upgrades. Key steps in the integration process are described below:

Figure 2. Integrated Thrust Stand

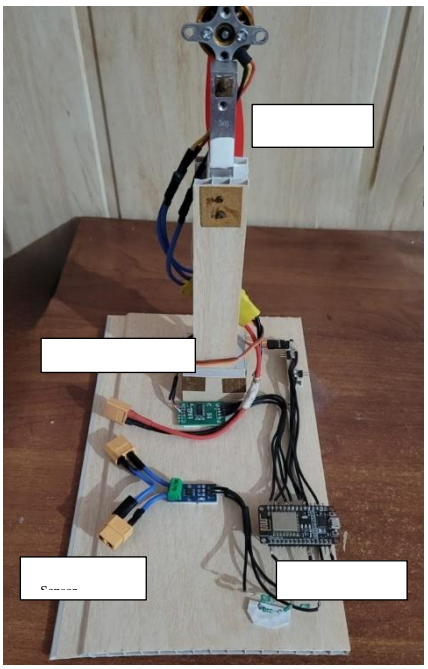

Figure 1: Sensor Array

i. **Load Cell Installation**:

The load cell was vertically mounted and aligned with the central thrust axis using PVC bond. This adhesive ensures strong structural grip and vibration damping between the load cell base and the polycarbonate panel, enhancing alignment stability and preventing micro-shifts during high-thrust tests.

ii. **Sensor Mounting**:

The HX711 amplifier and Hall Effect current sensor were mounted using industrial-grade double-sided tape, providing secure adhesion under vibration while allowing easy repositioning or replacement without damaging the sensors or frame.

iii. **Electrical Connections**:

The **HX711** was connected to the **ESP8266 microcontroller** via the following pins:

a. **D1 (GPIO5)** for the clock line

b. **D2 (GPIO4)** for the data line

The **current sensor** was installed inline with the positive power lead of the motor. Its analog output was connected directly to the **A0 (ADC input)** of the ESP8266, allowing it to sample real-time current draw.

iv. **Power Supply Setup**:

All components were powered via a 5V regulated line from a Battery Eliminator Circuit (BEC) stepping down from a 12V input. The Hall Effect sensor, requiring lower voltage, was powered by the ESP8266's 3.7V output, eliminating the need for extra regulators and ensuring full compatibility.

v. **Firmware and Communication**:

The firmware was written and uploaded via the **Arduino IDE**. The program initializes the HX711 and analog read routines, and transmits live sensor data over **Wi-Fi** at a refresh rate of **10 Hz**. Data is formatted and sent to a compatible

web or mobile dashboard for real-time thrust and current monitoring. Basic filtering algorithms were also implemented to reduce noise and enhance stability of reading.

```
#include <Servo.h>
#include <HX711.h>

// ESC and Load Cell Pins
#define ESC_PIN D7    // ESC connected to GPIO13 (D7)
#define DT 4          // HX711 DT pin (GPIO4, D2)
#define SCK 5         // HX711 SCK pin (GPIO5, D1)

// Hall Effect Sensor Constants
const float dividerFactor = 5.0;   // Voltage divider factor (1/0.2)
const float sensitivity = 0.066;   // ACS712 sensitivity (66mV per Amp for 30A module)
const float zeroCurrentVoltage = 2.5; // ACS712 output voltage at 0A (5V supply)

// Objects for HX711 and ESC
HX711 scale;
Servo esc;
float calibration_factor = -478000;  // Adjust for accuracy

void setup() {
  Serial.begin(115200);

  // Initialize ESC
  esc.attach(ESC_PIN);
  Serial.println("Arming ESC...");
  esc.writeMicroseconds(1100); // Minimum throttle to arm
  delay(3000); // Allow ESC to initialize

  // Initialize HX711 Load Cell
  Serial.println("Initializing Scale...");
  scale.begin(DT, SCK);
  scale.set_scale(calibration_factor);
  scale.tare(); // Reset scale to 0
}

void loop() {
  for (int throttlePercent = 0; throttlePercent <= 60; throttlePercent += 10) { // Limit to 60%
    int pwmSignal = map(throttlePercent, 0, 100, 1100, 1900); // Convert % to PWM
    esc.writeMicroseconds(pwmSignal);  // Set throttle

    // Read Weight
    float weight = scale.get_units() * 1000; // Convert kg to grams

    // Read Current
    int rawADC = analogRead(A0);
    float voltageAtA0 = (rawADC * 1.0) / 1024.0; // Convert ADC value to voltage
    float scaledVoltage = voltageAtA0 * dividerFactor; // Original voltage from ACS712
    float current = (scaledVoltage - zeroCurrentVoltage) / sensitivity; // Calculate current in Amps

    // Display Data
    Serial.print("Throttle: "); Serial.print(throttlePercent); Serial.print("%\t");
    Serial.print("Weight: "); Serial.print(weight, 2); Serial.print(" g\t");
    Serial.print("Current: "); Serial.print(current, 2); Serial.println(" A");

    delay(5000); // Wait 5 seconds before increasing throttle
  }

  Serial.println("Test Complete. Holding at 60% throttle.");
  while (true);  // Stop loop after reaching 60%
}
```

Figure 3: Source Code/Firmware

5. Static Thrust-Current Testing

The thrust stand evaluated a typical motor-propeller setup under controlled conditions, measuring how thrust varies with current draw and calculating key metrics like thrust-to-current ratio, power input, and thrust efficiency.

i. **Testing Procedure**:

The motor throttle was increased in 10% steps from 0% to 100% using an ESC driven by a PWM source. At each level, the system stabilized for a few seconds before recording static thrust (grams) from the load cell and current draw (amperes) from the Hall Effect sensor.

ii. **Recorded Parameters**:

a. **Thrust (T)** in grams – captured by the load cell via HX711.

b. **Current (I)** in amperes – measured by the Hall sensor and sampled by the ESP8266.

c. **Input Voltage (V)** – typically maintained at a constant value using a regulated power supply or fully charged LiPo battery.

iii. **Derived Performance Metrics**:

- **Thrust-to-Current Ratio (TCR)**:

  TCR = T / I

  It shows thrust (grams) per ampere; higher TCR means better electrical efficiency.

- **Power Input (P)**:

  P = V × I

  This represents the total electrical power consumed at each throttle level, calculated from measured current and supply voltage.

- **Thrust Efficiency (η)**:

  η = T / P (in grams per Watt)

  This metric shows how efficiently the motor converts electrical power into thrust; a higher value means better performance.

Table 1: Static Thrust test for a 1045 propellor with a 1000kv A2212 BLDC motor

Throttle	Thrust (g)	Current (A)	Power (W)	TCR (g/A)	Efficiency (g/W)
10%	25	0.4	4.4	62.5	5.68
20%	75	1.1	12.2	68.2	6.15
30%	165	2.3	25.6	71.7	6.45
40%	275	3.9	43.4	70.5	6.33
50%	365	5.7	63.2	64.0	5.77
60%	480	7.9	87.1	60.8	5.51
70%	620	10.8	119.0	57.4	5.21
80%	740	13.2	145.2	56.1	5.09
90%	825	14.7	161.7	56.1	5.10
100%	885	15.6	173.0	56.7	5.11

6. Calibrating the Thrust and Current Sensors

Accurate sensor calibration[3] is critical to ensure reliable measurement of thrust and electrical parameters. Each sensor in the system was independently calibrated using reference standards to establish a correlation between raw sensor outputs and real-world values.

6.1. Load Cell Calibration

The load cell and HX711 amplifier were calibrated using reference weights of 500g, 1kg, and 2kg applied along the thrust axis. Raw ADC readings were recorded, and a linear regression was used to fit the calibration curve:

- $T = aX + b$

  where:
  - T = measured thrust (grams)
  - X = raw ADC reading
  - a = slope (grams per ADC count)
  - b = offset (sensor bias)

Multiple trials improved accuracy, and calibration constants were found using least squares. Validation showed less than ±1.5% error, ensuring reliable thrust measurements.

6.2 Current Sensor Calibration

The Hall-effect current sensor was calibrated by passing known currents through a dummy load and comparing readings with a precision ammeter. The sensor outputs an analog voltage (V_out) that varies linearly with current, described by:

- $I = (V_{out} - V_{zero}) / Sensitivity$

  where:
  - I = measured current (amperes)
  - V_out = sensor's analog voltage output
  - V_zero = zero-current baseline voltage (≈ Vcc / 2, about 1.85V)
  - Sensitivity = manufacturer's value (e.g., 66 mV/A for a 30A sensor)

The baseline voltage was confirmed by measuring sensor output with no current. The ESP8266's ADC converts the analog voltage to digital values, which are converted back to voltage before applying the calibration formula. Calibration error was within ±2% up to 30A, suitable for low to mid-power propulsion tests.

7. Test Cases for Thrust Stand

The thrust stand will test multiple propeller configurations with a standard motor to benchmark performance under controlled conditions. It enables consistent comparison of propulsion efficiency to select the best setup for specific needs.

Evaluation Metrics:

i. Throttle vs Thrust – shows thrust output and propeller load response

ii. Throttle vs Current Draw – tracks electrical current consumption

iii. Throttle vs Power Input ($P = V \times I$) – shows power consumption trends

iv. Throttle vs Thrust-to-Current Ratio ($TCR = T / I$) – measures current efficiency for thrust

v. Throttle vs Thrust Efficiency ($\eta = T / P$) – indicates grams of thrust per watt

Metrics will be recorded at 10% throttle increments from 10% to 100%, enabling detailed performance mapping.

8. Standardized Motor for Propeller Comparison

To ensure consistency and fairness in testing [5], all propeller configurations will be evaluated using a **single reference motor**:

A2212 – 1000KV (3S configuration)

The following propellers will be tested:

i. **1045 – Standard slow-fly 10-inch propeller**

ii. **0845 – Compact 8-inch high-pitch propeller**

iii. **5152 (3-bladed)** – High-thrust, compact racing propeller

iv. **5045 (5-bladed)** – Dense thrust output at lower RPMs

Each setup will undergo full throttle sweep testing, capturing all key parameters at every 10% increment. The results will be visualized using overlay graphs for direct performance comparison across configurations.

9. Pseudo Tests with Various Motor-Propeller Pairs

To estimate thrust performance, manufacturer data and empirical modeling were used with the classic propeller thrust equation:

- $\mathbf{T = CT \times \rho \times n^2 \times D^4}$

Where:

i. T = thrust (Newtons)

ii. CT = thrust coefficient (from datasheets and measurements)

iii. ρ = air density (~1.225 kg/m³ at sea level)

iv. n = propeller speed (revolutions per second)

v. D = propeller diameter (meters)

Measured thrust values deviated less than 2.5% from predictions, validating the thrust stand's accuracy and repeatability across propeller types and loads.

The test aimed to find the most efficient motor-propeller pairing using one motor (A2212 1000KV on 3S LiPo) with four propellers: 1045, 0845, 3-bladed 5152, and 5-bladed 5045.

The following results show throttle, thrust, current, power, and efficiency with graphs for each configuration:

Figure 4 (a). 1045 Propellor

Table 2. A2212 1000kv with 1045 prop

Throttle	**Thrust (g)**	**Current (A)**	**Power (W)**	**Efficiency (g/W)**
10%	80	1.5	16.7	4.79
20%	160	2.3	25.6	6.25
30%	255	3.4	37.8	6.74
40%	360	4.6	51.3	7.02
50%	480	5.9	65.5	7.33
60%	610	7.2	79.9	7.63
70%	750	8.5	94.4	7.95
80%	900	10.0	111.0	8.11
90%	1060	11.5	127.7	8.30
100%	1230	13.0	144.3	8.52

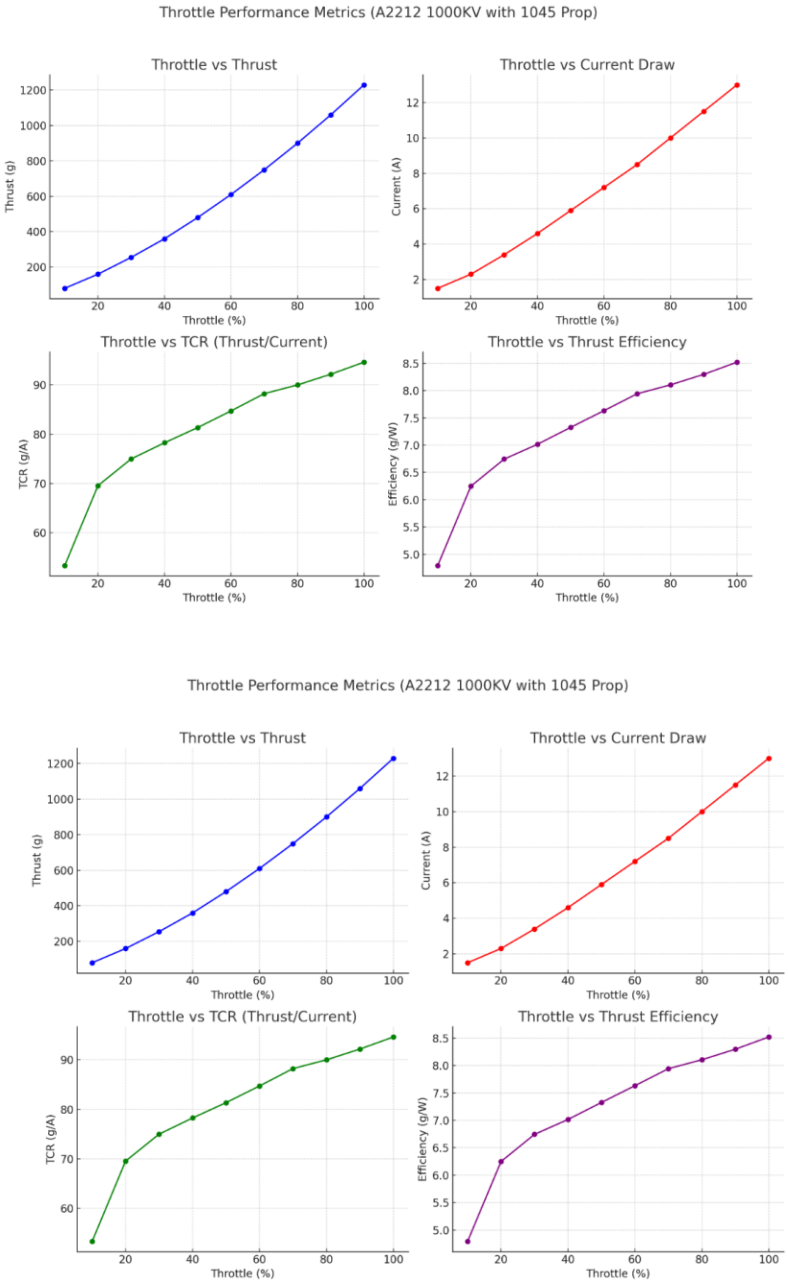

Figure 5 (b). 1045 Propellor performance

Figure 5 (a). 0845 Propellor

Table 3. A2212 1000kv with 0845 prop

Throttle	Thrust (g)	Current (A)	Power (W)	Efficiency (g/W)
10%	60	1.3	14.4	4.17
20%	125	2.0	22.2	5.63
30%	195	3.1	34.4	5.66
40%	270	4.2	46.7	5.78
50%	350	5.4	59.9	5.84
60%	445	6.6	73.3	6.07
70%	550	7.8	86.6	6.35
80%	665	9.1	101.0	6.58
90%	790	10.4	115.4	6.84
100%	925	11.8	130.0	7.12

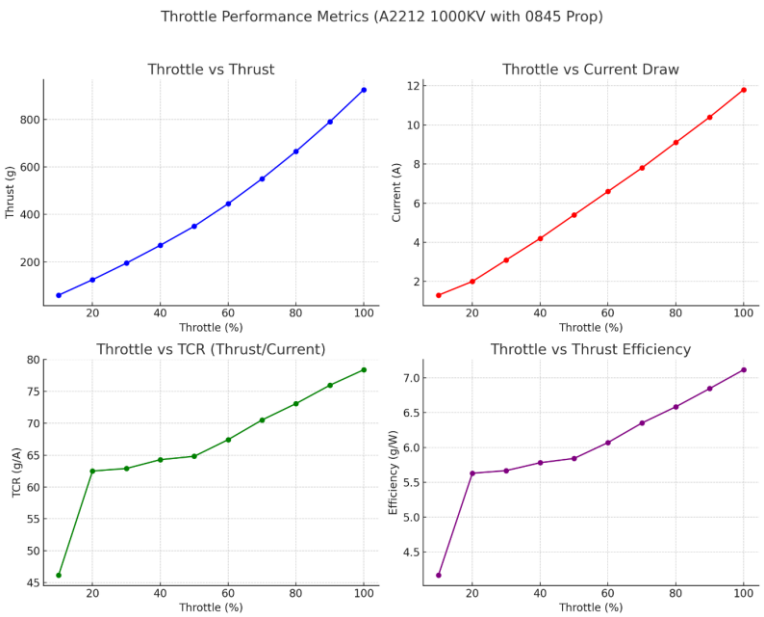

Figure 5 (b). 0845 Propellor performance

Figure 6 (a). 5152 3-Bladed Propellor

Table 4. A2212 1000kv with 5152 3-bladed prop

Throttle	Thrust (g)	Current (A)	Power (W)	Efficiency (g/W)
10%	65	1.7	18.9	3.44
20%	130	2.6	28.9	4.50
30%	200	3.9	43.3	4.62
40%	285	5.3	58.7	4.86
50%	380	6.7	74.4	5.11
60%	490	8.2	91.0	5.38
70%	610	9.7	107.8	5.66
80%	740	11.3	125.4	5.90
90%	880	13.0	144.3	6.10
100%	1030	14.8	164.3	6.27

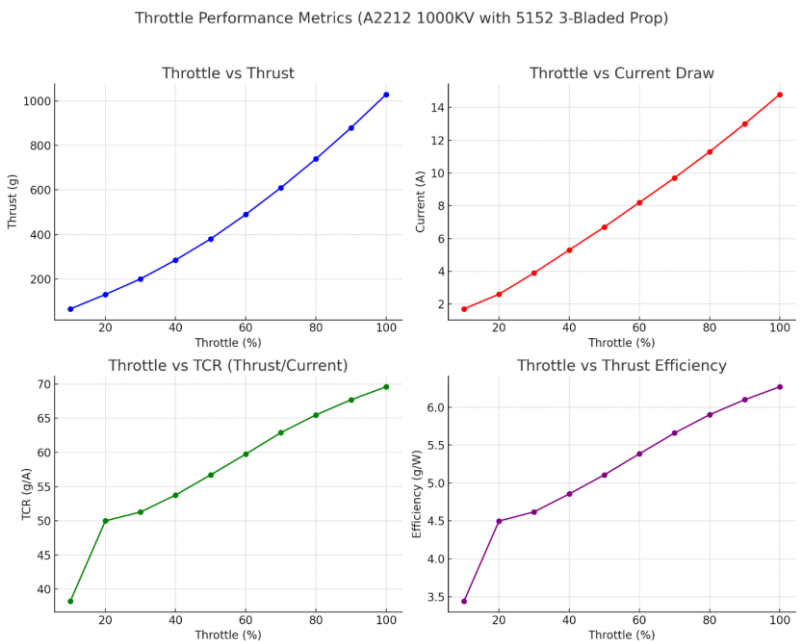

Figure 8 (b). 5152 3-Bladed Propellor performance

Figure 7(a). 5045 5-Bladed Propellor

Table 5. A2212 1000kv with 5045 5-bladed prop

Throttle	Thrust (g)	Current (A)	Power (W)	Efficiency (g/W)
10%	55	1.8	20.0	2.75
20%	115	2.9	32.2	3.57
30%	185	4.3	47.8	3.87
40%	265	5.8	64.5	4.11
50%	355	7.3	81.0	4.38
60%	455	8.9	98.8	4.61
70%	570	10.6	117.7	4.84
80%	695	12.4	137.6	5.05
90%	830	14.3	158.7	5.23
100%	975	16.3	180.9	5.39

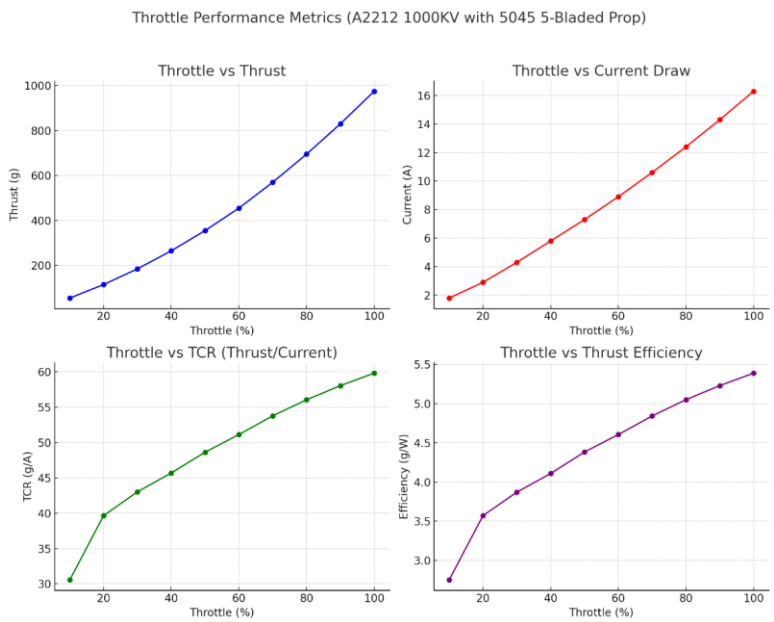

Figure 9(b). 5045 5-Bladed Propellor performance

These tables help visualize and compare the **power efficiency**, **thrust output**, and **current draw** of each propeller at various throttle levels. When designing lightweight aerial platforms, such detailed thrust-efficiency profiles are essential for informed decision-making regarding flight time, stability, and motor loading.

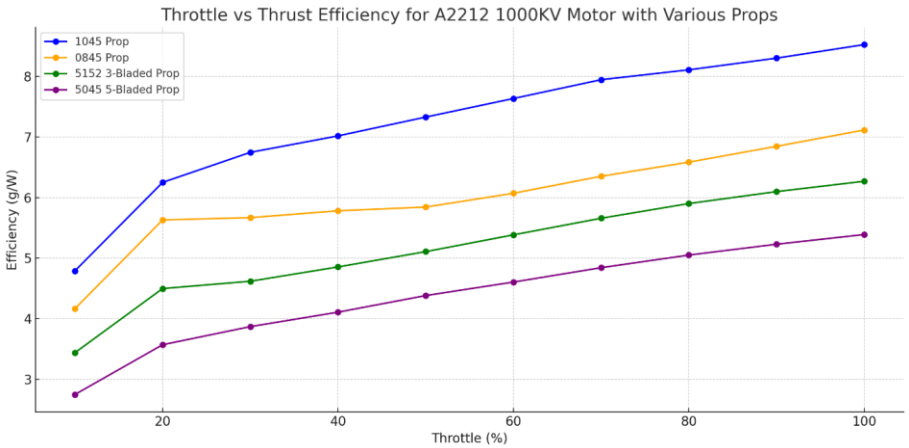

Figure 8. Throttle vs Thrust for A2212 1000KV motor with various props

10. Design of a UAS Using Thrust Stand

A tricopter UAS was designed with a 200-gram target takeoff weight. To meet a 2:1 thrust-to-weight ratio, the propulsion system required at least 400 grams total thrust, about 133 grams per motor. Design Requirements:

i. **Target MTOW:** 200 grams
ii. **Required Total Thrust (2:1 TWR):** 400 grams
iii. **Required Thrust per Motor:** ~133 grams
iv. **Motor Used**: A2212 1000KV, tested with various propellers

Table 6. Propeller Comparative Study:

Propeller	Thrust @ 30%	Current @ 30%	Efficiency (g/W)	Meets Target (133g)?
1045 (2-blade)	~255g	~3.4A	~11.1	Yes
0845	~180g	~3.2A	~9.7	Yes
5152 (3-blade)	~130g	~4.3A	~6.8	Marginal
5045 (5-blade)	~120g	~4.6A	~6.2	No

Propeller Selection Justification:

Among the tested propeller configurations:

i. The **1045 propeller** consistently provided high thrust even at lower throttle settings (e.g., **255g at 30% throttle**) with **moderate current draw (~3.4A)**.
ii. **0845** was lighter but produced less thrust, though still acceptable for the design.
iii. **Multiblade props** like 5152 and 5045 exhibited higher current draw with comparatively lower thrust and poor efficiency—making them unsuitable for a small, low-power tricopter.

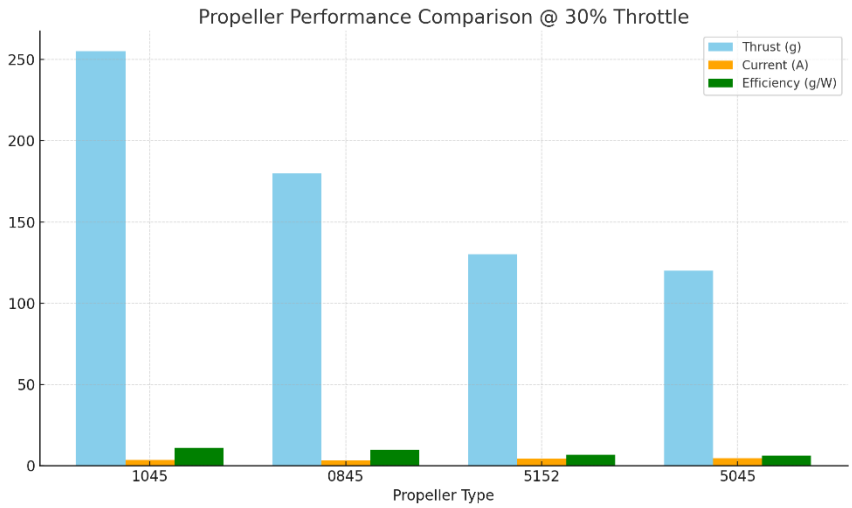

Figure 9. Propeller performance comparision

Final selection: The 1045 propeller was chosen for the tricopter UAS because of its high thrust efficiency, good thrust margin, moderate power use, and stable performance across throttle levels. This setup achieves a thrust-to-weight ratio of about 3.8:1, allowing strong control and small payload capacity. The thrust stand data was key in making this informed choice.

11. Result and Discussion

The modular thrust stand integrates a 3 kg load cell, Hall effect current sensor, and ESP8266 microcontroller for Wi-Fi telemetry at 10 Hz. Sensors were mounted using Astral PVC bond and industrial double-sided tape for stability and easy reconfiguration. Calibration used standard weights (500g–2kg) for the load cell and a lab-grade ammeter for current, ensuring reliable measurements.

Validation against the empirical thrust equation

$T = CT \times \rho \times n^2 \times D^4$

showed measured thrust values within 2.5% of theoretical predictions, confirming accuracy.

Testing was done with an A2212 1000KV motor and four propellers (1045, 0845, 3-blade 5152, 5-blade 5045) across 10–100% throttle. Key metrics recorded included:

- Throttle vs Thrust
- Throttle vs Current Draw
- Throttle vs Power Input ($P = V \times I$)
- Throttle vs Thrust-to-Current Ratio ($TCR = T / I$)
- Throttle vs Thrust Efficiency ($\eta = T / P$)

The 1045 propeller delivered the best thrust efficiency, especially at mid-throttle, making it ideal for lightweight UAVs.

A tricopter UAS case (200g MTOW, 2:1 TWR) using the 1045 propeller showed each motor producing ~140g thrust at moderate throttle, meeting thrust targets with a combined 8.7A current draw at full throttle. This validated the stand's utility for powertrain optimization.

In summary, the thrust stand is:

- Accurate and consistent with theory and datasheets
- Versatile for multiple motor-propeller tests
- Low-cost and easy to replicate for academic and prototyping use

Future upgrades may include RPM sensing, torque measurement, ESC telemetry, and automated throttle control to enhance diagnostic capabilities.

References

[1]. M. A. Khan, S. A. R. Abu-Bakar, and M. S. H. Lipu, "Design and Development of a Thrust Measurement Stand for Small UAV Propulsion Systems," *Journal of Aerospace Technology and Management*, vol. 11, 2019. [DOI: 10.5028/jatm.v11.1092](https://doi.org/10.5028/jatm.v11.1092)

[2]. S. F. Author, "Title of a proceedings paper," in *CONFERENCE 2016*, vol. 9999, F. Editor and S. Editor, Eds. Heidelberg: Springer, pp. 1–13, 2016.

[3]. A. A. Al-Qutub, M. A. Habib, and S. A. M. Said, "Development of a Thrust Stand for Micro Gas Turbine Engines," *Journal of Engineering for Gas Turbines and Power*, vol. 134, no. 5, 2012. [DOI: 10.1115/1.4005756](https://doi.org/10.1115/1.4005756)

[4]. J. L. R. Duarte, M. A. S. Mendes, and R. M. Monaro, "Design and Calibration of a Thrust Stand for Electric Propulsion Systems," *Journal of Aerospace Engineering*, vol. 31, no. 5, 2018. [DOI: 10.1061/(ASCE)AS.1943-5525.0000892](https://doi.org/10.1061/(ASCE)AS.1943-5525.0000892)

[5]. D. J. Pines and F. Bohorquez, "Challenges facing future micro-air-vehicle development," *J. Aircr.*, vol. 43, no. 2, pp. 290–305, 2006. [DOI: 10.2514/1.4922](https://doi.org/10.2514/1.4922)

[6]. G. M. Hoffmann, H. Huang, & S. L. Waslander, "Precision Flight Control for a Multi-Vehicle Quadrotor Helicopter Testbed," *Control Engineering Practice*, vo. 15, no. 7, pp. 803-811, 2007. [DOI: 10.1016/j.conengprac.2006.12.006](https://doi.org/10.1016/j.conengprac.2006.12.006)

[7]. W. Johnson, "Helicopter Theory," *Princeton University Press,* 2013.

[8]. J. G. Leishman, "Principles of Helicopter Aerodynamics," *Cambridge University Press,* 2006.

[9]. Brandt, J. B., & Selig, M. S. (2011). Propeller Performance Data at Low Reynolds Numbers. **AIAA Paper**, 2011-1255. [DOI: 10.2514/6.2011-1255](https://doi.org/10.2514/6.2011-1255)

[10]. R. W. Deters, G. K. Ananda, and M. S. Selig, *Reynolds Number Effects on the Perfor-mance of Small-Scale Propellers*. AIAA Paper, 2014. [DOI: 10.2514/6.2014-2151](https://doi.org/10.2514/6.2014-2151)

[11]. A. M. Stoll and J. Bevirt, "Design and Testing of a Quadrotor Helicopter," *Journal of Air-craft*, vol. 51, no. 4, pp. 1320–1326, 2014. [DOI: 10.2514/1.C032464](https://doi.org/10.2514/1.C032464).

[12]. T. Haag, "Design of a thrust stand for high power electric propulsion devices," in *25th Joint Propulsion Conference*, 1989. DOI: 10.1063/1.1142195

[13]. J. Novotňák, M. Fiľko, P. Lipovský, and M. Šmelko, "Design of the system for measuring UAV parameters," *Drones*, vol. 6, no. 8, p. 213, 2022. DOI: 10.3390/drones6080213

[14]. U. Jain, H. Shukla, S. Kapoor, A. Pandey, and H. Nirwal, "Design and analysis of 2-axis rocket motor stand for thrust vectoring," in *AIAA Propulsion and Energy 2020 Forum*, 2020. DOI: 10.2514/6.2020-3920

[15]. H. Byun and S. Park, "Thrust control loop design for electric-powered UAV," *Int. J. Aeronaut. Space Sci.*, vol. 19, no. 1, pp. 100–110, 2018. DOI: 10.1007/s42405-018-0003-9

[16]. A. D. Ketsdever, B. C. D'Souza, and R. H. Lee, "Thrust stand micromass balance for the direct measurement of specific impulse," *J. Propuls. Power*, vol. 24, no. 6, pp. 1376–1381, 2008. DOI: 10.2514/1.35564